journal

J. Am. Ceram. Soc., 87 [9] 1669–1676 (2004)

Preparation of YBCO Films on CeO_2-Buffered (001) YSZ Substrates by a Non-Fluorine MOD Method

Y. Xu,[†,‡,§] A. Goyal,[*,‡] J. Lian,[¶] N. A. Rutter,[‡] D. Shi,[*,§] S. Sathyamurthy,[*,††] M. Paranthaman,[*,††] L. Wang,[*,¶] P. M. Martin,[‡] and D. M. Kroeger[‡]

Metals and Ceramics Division, Oak Ridge National Laboratory, Oak Ridge, Tennessee 37831

Department of Materials Science, University of Cincinnati, Cincinnati, Ohio 45221

Department of Nuclear Engineering and Radiological Science, University of Michigan, Ann Arbor, Michigan 48109

Chemical Science Division, Oak Ridge National Laboratory, Oak Ridge, Tennessee 37831

$YBa_2Cu_3O_{7-\delta}$ (YBCO) films were fabricated via a fluorine-free metal organic deposition (MOD) method followed by high-temperature, low oxygen partial pressure annealing. Trimethyl acetate salts of copper, yttrium, and barium hydroxide were used as the precursors, which were dissolved in proponic acid- and amine-based solvents. After spin-coating and burnout, samples were annealed at 740°C in 180 ppm oxygen partial pressure and exposed to humid atmosphere for different times. A critical transition temperature, $T_c(R=0)$ of 90.2 K and a transport critical current density (J_c) of 0.55 MA/cm^2 (77 K and self-field) were obtained for 0.2 μm YBCO films on CeO_2-buffered yttria-stabilized zirconia (YSZ) substrates. X-ray studies shows that the YBCO films have sharp in-plane and out-of-plane texture for all samples; however, the porosity of the YBCO film varies with the time of exposure to the humid atmosphere. A reaction between YBCO and CeO_2 during the high-temperature anneals and formation of the reaction product $BaCeO_3$ was confirmed by X-ray diffraction (XRD) studies. The XRD and transmission electron microscopy analysis indicated that the epitaxial relations in the film were YBCO (00*l*)//CeO_2 (00*l*)//YSZ (00*l*) and YBCO [100]//CeO_2 [110]//YSZ [110].

I. Introduction

COMPARED with processes such as pulsed laser deposition (PLD), e-beam co-evaporation, sputtering, and other popular physical methods, metal organic deposition (MOD) is a non-vacuum method and has such favorable features as precise composition control, high speed, low cost, and scalability for industrial production. In the MOD methods, various precursors such as acetates, citrates, oxalates, neodecanoates, trifluoroacetates, halides, acetylacetonates, and naphthenates have been described in the literature.[1–4] Furthermore, a recent overview of previous attempts at $YBa_2Cu_3O_{7-\delta}$ (YBCO) film fabrication using non-fluorine-based bulk solution techniques finds that no previous report of high-J_c film fabrication using fluorine-free precursors.[5] The interest in fluorine-containing precursors for YBCO films began when it was noted that such solutions decompose to carbonate-free precursor films, rather than films that contain substantial amounts of barium carbonate.[6–9] Recently, the fabrication of $YBa_2Cu_3O_{7-\delta}$ films through the TFA-MOD (trifluoroacetate metal organic deposition) approach[6,7] has become popular because high J_c has been demonstrated on lattice-matched single crystalline substrates[7,10,11] and also on metallic substrates such as RABiTS.[12–16] In a fluorine-free MOD process, it was believed that during the YBCO phase growth, certain metal organic precursors could lead to barium carbonate as an intermediate phase due to the formation of carbon dioxide during processing of the carbon-containing precursor ligands attached to the barium ions. Usually, the ligand is removed by hydrolysis with excess water followed by precipitation of the resulting barium hydroxide. However, fatty acid ester ligands cannot be removed by simple oxidation or hydrolysis. It is necessary to process YBCO films above 900°C to decompose the intermediate barium carbonate, which can interfere kinetically with the formation of the YBCO phase.[17,18] For these reasons, non-carbon-containing precursors are preferred.

However, our experiments show that the formation of barium carbonate is really a processing-related intermediate product.[19] For the first time we introduced water vapor during the high-temperature conversion of fluorine-free precursors and obtained a high current density over 1 MA/cm^2.[19] With this novel processing method, no barium carbonate was detected. Our previous work focused on STO and LAO substrates. Since most substrates being scaled up for coated conductors have a CeO_2 cap layer on yttria-stabilized zirconia (YSZ) buffer layers, this work focuses on CeO_2-buffered YSZ substrates.

II. Experimental Procedure

The trimethyl acetate and proponic acid precursor solution was prepared by dissolving trimethyl acetates of Y and Cu together with barium hydroxide into proponic acid in a 1:2:3 cation ratio. Amine was added to increase the solubility and adjust the viscosity, while the addition of xylene was used to control the wetting and oxide content in the solution. The viscosity was normally adjusted in the range of 30–100 cP, and the oxide content was around 7–10 wt%. The total ionic concentration was 0.5–1.0 mol/L. YSZ single crystals ($15 \times 3 \times 0.5$ mm^3) with (001) orientation were used as substrates. CeO_2 was sputtered onto the YSZ substrate to form a cap layer with the same orientation. YBCO films were prepared by spin-coating at 3000 rpm for 30 s. Multiple coatings were required for thicker films. The green films were then dried at 200°C for 4–5 min in air on a hot plate. Each coating generally gave a thickness of about 100 nm. The gel films formed on the hot plate were then burned out at 400°C in humid oxygen. The high-temperature annealing was conducted at 700°–

R. K. Bordia—contributing editor

Manuscript No. 10328. Received June 21, 2003; approved December 8, 2003.
This research was sponsored by the United States Department of Energy, Office of Energy Efficiency and Renewable Energy, Office of Distributed Energy and Electric Reliability-Superconductivity program. This research was performed at the Oak Ridge National Laboratory, managed by UT-Battelle, LLC for the United States Department of Energy under Contract No. DE-AC05-00OR22725.

[*]Member, American Ceramic Society.
[†]To whom correspondence should be addressed. e-mail: xuy@ornl.gov.
[‡]Metals and Ceramics Division, Oak Ridge National Laboratory.
[§]University of Cincinnati.
[¶]University of Michigan.
[††]Chemical Science Division, Oak Ridge National Laboratory.

Table I. Processing Parameters and Electrical Properties of YBCO Films Derived from the TMAP Approach

Sample ID[†]	$P(O_2)$ (ppm)	Dew point (°C)	T_{ann} (°C)	Wet-dwell[†] (min)	T_c (0) (K)	ΔT_c[‡] (°C)	J_c (MA/cm^2)	YBCO (005) FWHM[§] (deg)	ρ_{285}/ρ_{100}[¶]
a	180	35	740	57	88.8	2.5	0.25	1.31	1.93
b	180	35	740	45	90.2	2.4	0.35	1.18	2.28
c	180	35	740	30	90.2	1.6	0.55	1.73	2.51
d	180	35	740	10	88.3	3.0	0.35	1.68	2.51

[†]Wet-dwell references the dwell time in humid atmosphere at 740°C. After a wet-dwell, the humid furnace gas is changed to dry. The total holding time at 740°C is 1 h for this set of experiments. [‡]Transition temperature, the temperature interval from the transition start to the temperature where resistance drops to zero. [§]Full width at half-maximum. [¶]Ratio of resistivity at 285 K to that at 100 K.

860°C for 1 h in a quartz tube furnace, first in humid atmosphere and then a dry atmosphere. Normally, the 180 ppm oxygen partial pressure was read by a zirconium oxygen sensor. Silver contacts around 1 μm in thickness were sputtered onto the YBCO samples at room temperature before oxygen annealing. The oxidation was performed at 400°–500°C for 1 h followed by a cooling ramp of 2°C/min to 350°C to diffuse oxygen into the YBCO perovskite structure and to establish good contact of Ag with the YBCO film. T_c and the critical current (I_c) were measured by the direct four-probe transport method. Surface morphologies were observed by scanning electron microscopy (SEM). Cross-sectional structure and interface were examined with high-resolution transmission electron microscope (HRTEM) and selected area diffraction (SAD). Thickness and film stoichiometry was determined by Rutherford backscattering spectroscopy (RBS). Characterization of the films and their texture were examined using X-ray diffraction (XRD) through θ–2θ scans, ω-scans, ϕ-scans, and pole figures.

III. Results and Discussions

In this research, the effect of the wet-dwell time on electrical transport properties, the texture of YBCO films, the interface structure of YBCO/CeO_2/YSZ, and film morphologies was investigated for the samples annealed at 740°C for 1 h in 180 ppm oxygen partial pressure. The dependence of $T_c(R=0)$, ΔT_c, J_c, full width at half-maximum (FWHM) of YBCO (005) ω-scan, and ρ_{285}/ρ_{100} on wet-dwell time are listed in Table I. Experimental data clearly show that J_c values are strongly related to the dwell time in humid furnace gas, and the highest J_c value of the YBCO film on CeO_2-buffered YSZ substrate was obtained for the sample with a wet-dwell time of 30 min. Other properties such as $T_c(R=0)$, ΔT_c, FWHM, and ρ_{285}/ρ_{100} are also directly related to the dwell time in humid atmosphere.

To investigate the phase development, XRD θ–2θ scans of YBCO films, as shown in Fig. 1, were performed on samples annealed for different dwell times in humid atmosphere. The diffraction patterns of the samples examined in this study did not change dramatically with wet-dwell time except the differences in intensities. For all the films produced under different dwell times in wet gas, only the (00*l*) orthorhombic YBCO reflections were observed. Peaks from substrate, buffer layer, and reaction product, such as the peaks of (002) YSZ and (002) CeO_2, and peaks of (110) and (002) reflections associated with the reaction product of $BaCeO_3$ were also observed. No other reflections for either YBCO or any other phase were detected. For the fluorine-free method, the residual $BaCO_3$ may ruin the electrical properties of YBCO films. XRD θ–2θ scans do not contain either the cubic (200) peak at 25.57° (100%) or orthorhombic (111) peaks at 23.9° (100%) of $BaCO_3$, demonstrating that all the intermediate phases in the precursor films are fully converted. We were unable to detect the peaks of YBCO (013), (103), and (213) peaks at 32.5°, 32.8°, and 58.2°, respectively, which would represent polycrystalline YBCO film; hence, there is good nucleation and epigrowth of the YBCO film on CeO_2-buffered YSZ single-crystal substrates. Some *a*-oriented growth (a (200) peak at 47.58°) is observed but compared with YBCO (006), its intensity is very low ($I_{200} < 200$ counts and $I_{200}/I_{006} < 1.5\%$). As shown in Fig. 1, the intensity of the YBCO (00*l*) reflections strongly relate to the wet-dwell time. Shorter (10 min) or longer (57 min) dwells in humid furnace gas result in relatively low intensity of YBCO (00*l*) peaks in the XRD θ–2θ scans. The highest intensity is observed for a wet-dwell time of around 30−45 min. The results are consistent with that of $T_c(R=0)$, ΔT_c, and J_c measurements.

The out-of-plane and in-plane textures of YBCO films were further investigated by ω-scans, ϕ-scans, and pole figures, as shown in Figs. 2–4, respectively. The FWHM data of YBCO (005) ω-scans (Fig. 2), as determined by a fitted gaussian to the

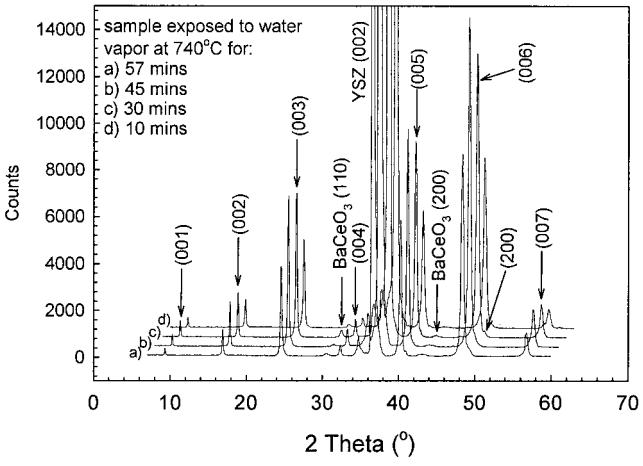

Fig. 1. X-ray θ–2θ reflections of YBCO film on CeO_2-buffered YSZ substrate. Samples were converted at 740°C in 180 ppm oxygen for 60 min. The time exposed to water vapor at 740°C was (a) 57, (b) 45, (c) 30, and (d) 10 min, respectively.

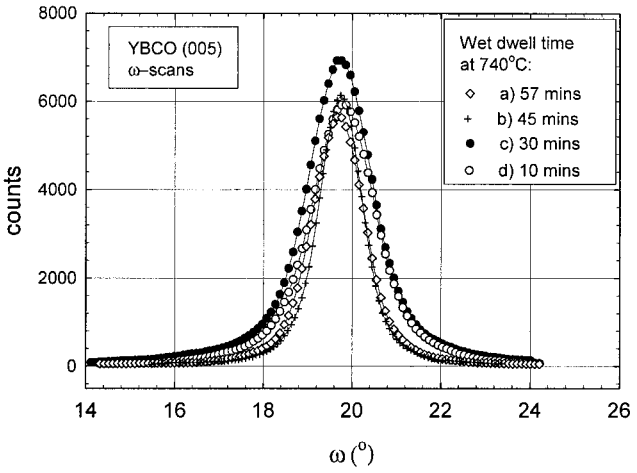

Fig. 2. Rocking curves of the YBCO (005) plane. These show the good out-of-plane texture of the sample annealed at 740°C in 180 ppm oxygen pressure with different wet-dwell times.

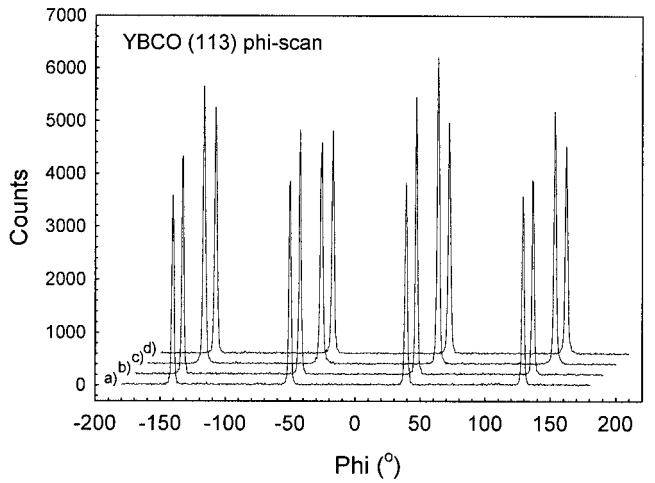

Fig. 3. X-ray ϕ-scans of YBCO (113) plane for samples annealed at 740°C in 180 ppm oxygen pressure with different wet-dwell times, indicating good in-plane texture for all of the samples: (a) 57, (b) 45, (c) 30, and (d) 10 min, respectively.

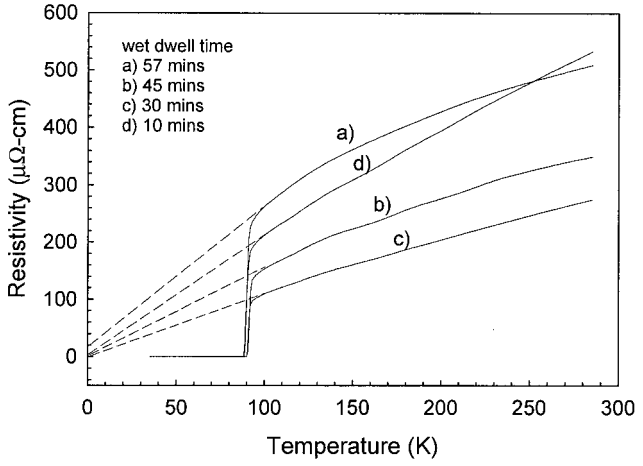

Fig. 5. Four-probe measurement of the temperature dependence of the electrical resistivity for samples annealed at 740°C in 180 ppm oxygen pressure with different wet-dwell times. The short dashed lines show the extrapolation of the low-temperature part of the resistivity lines divided by the dashed line in the normal state.

experimental data, are listed in Table I. A high-quality out-of-plane and in-plane texture is achieved for all the investigated samples: ω- and ϕ-scans of these samples have FWHM values of $\Delta\omega = 1.2°–1.8°$ for the (005) reflections and $\Delta\phi = 1.8°–2.4°$ for the (113) reflections, respectively. No significant modifications of the texture quality with wet-dwell time were detected in these experiments and the results are comparable with that in XRD θ–2θ scans. However, as shown in Figs. 2 and 3, the sample annealed in the wet-dwell time of 30 min gives the highest intensity both in the ω-scan and ϕ-scans, demonstrating 30 min anneal in humid atmosphere resulted in the best developed texture, and the highest T_c, lowest ΔT_c and highest J_c.

To determine the exact orientation of the YBCO in the epitaxial film as well as the orientation of buffer and substrate, XRD pole-figure scans were obtained for the YBCO (113), CeO_2 (111), and YSZ (111) reflections. No observable difference was present among the YBCO films annealed for different wet-dwell times, and also there was no detectable difference among CeO_2 pole figures and YSZ pole figures. Fig. 4 shows a typical set of intensity–contour plots of these reflections. The YBCO pole figure (Fig. 4(c)) shows the standard four specific orientations for the (113) plane normal, demonstrating that the film is *c*-oriented with *a–b* in-plane alignment. The position of the YBCO (113) poles is 45° rotated about [001] relative to the CeO_2 (111) and substrate YSZ (111) poles.

The influence of the wet-dwell time can be clearly detected and quantified through measurements of the temperature dependence of the electrical resistivity in the normal state. Figure 5 displays $\rho(T)$ curves measured for films grown with different wet-dwell times. The residual resistivity, $\rho(0)$, remains essentially zero in these YBCO films. Also the transition temperature is found to be in all cases $T_c(R=0) \approx 88–90$ K. As it may be observed, both the room-temperature resistivity, $\rho(285)$, and the slope of $\rho(T)$ are enhanced in samples with shorter or longer dwells in the humid atmosphere. We should note that for the 30-min wet-dwell sample, the lowest resistivity $\rho(100\text{K}) \approx 108$ μΩ·cm and $\rho(285\text{K}) \approx 272$ μΩ·cm, together with the high-resistivity ratio $\rho(285\text{K})/\rho(100\text{K}) \geq 2.5$ and extrapolates to zero near 0 K. This is typical of high-quality, in-plane-aligned YBCO film with little grain-boundary scattering in the normal state and is observed for films grown through the vacuum process. Except for a relatively high T_c and sharp transition ($\Delta T_c = 1.62$ K), a linear behavior $\rho(T) = CT$ is observed for the sample annealed for 30 min in humid furnace gas. Though the resistivity ratio $\rho(285\text{K})/\rho(100\text{K})$ is high (≥2.5) for the 10-min wet-dwell sample, $T_c(R=0)$ is low (88.3 K) and the transition width ΔT_c is relatively broad (2.98 K); also $\rho(285\text{K})$ and

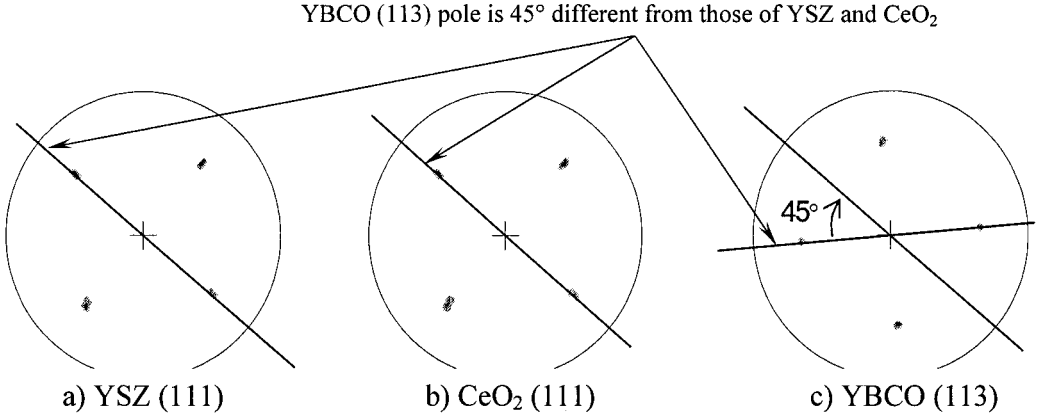

Fig. 4. Pole figures of YSZ (111), CeO_2 (111), and YBCO (113), showing a typical set of intensity–contour plots of these reflections. The standard four specific orientations for the (113) plane of YBCO film shows the *c*-oriented with *a–b* in-plane alignment in the film, the pole position of the YBCO (113) plane rotated 45° from those of CeO_2 (111), and/or the substrate YSZ (111) poles demonstrating the epitaxial growth alignment: YBCO (00*l*)//CeO_2 (00*l*)//YSZ (00*l*) and YBCO [100]//CeO_2 [110]//YSZ (110).

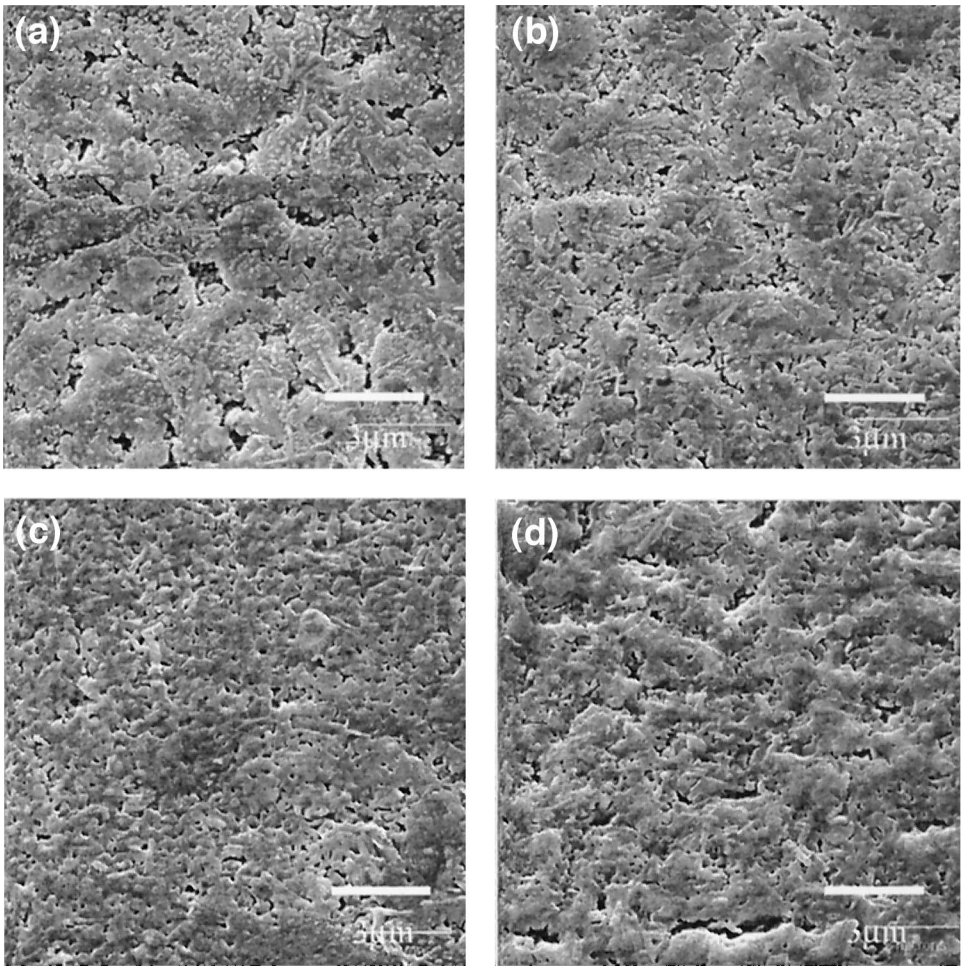

Fig. 6. SEM micrographs of TMAP-derived, 200-nm-thickness YBCO films annealed at 740°C in 180 ppm oxygen with different wet-dwell times: (a) 57, (b) 45, (c) 30, and (d) 10 min.

ρ(100K) are higher than those of sample (c). An even longer hold in humid furnace gas, sample (d), resulted in high normal state resistivity, a broad transition, low T_c, and the ρ(T) temperature dependence deviates from the linear behavior of a good YBCO film. The relatively high resistivity in the normal state, especially for samples (a), (b), and (d), may come from the porosity in the YBCO films as shown in scanning electron microscopy (SEM) top-view morphologies in Fig. 6. The resistivity was calculated under the assumption that a film is fully dense without pores or other defects at the intersection. But pores are unavoidable, especially for the MOD-derived films. We can then suggest that the enhanced resistivity, ρ(T), arises mainly from a reduction of the effective transport cross section. The statistical data are not available in this case; however, an estimate of the porosity from the SEM micrographs in Fig. 6 gives the decreasing sequence of porosity as $p_{(a)} > p_{(d)} > p_{(b)} > p_{(c)}$, which coincides with the normal-state resistivity sequence at 100 K: $\rho_{(a)} > \rho_{(d)} > \rho_{(b)} > \rho_{(c)}$, indicating that porosity may be an important factor contributing to the increased normal-state resistivity.

The transport properties at 77 K for the YBCO film annealed for 30 min in humid furnace gas are shown in Figs. 7 and 8 with magnetic field, H, applied parallel to the c-axis direction ($H//C_\perp$). An electric field criterion of 1 μV/cm was used in the J_c measurement. The dependence of self-field critical current densities on the wet-dwell time is shown in the inset of Fig. 8. J_c is calculated using the measured critical currents, the width of the YBCO film, and the nominal film thickness of 200 nm determined by Rutherford backscattering spectroscopy measurements. In self-field, the YBCO film annealed for 30 min in wet atmosphere had a J_c of 550 000 A/cm^2, around one-third of the critical current density achieved on LAO substrates.[19] The ratio of the current density at 0- and 0.5-T field $J_c(0T)/J_c(0.5T) = 2.4$, is smaller than the usually measured value of about 4. It is not clear why the J_c in self-field is low. It has been suggested that 90° grain boundaries associated with a-axis-oriented grains lead to a reduction of critical current density J_c by 2 orders of magnitude.[10] But in this

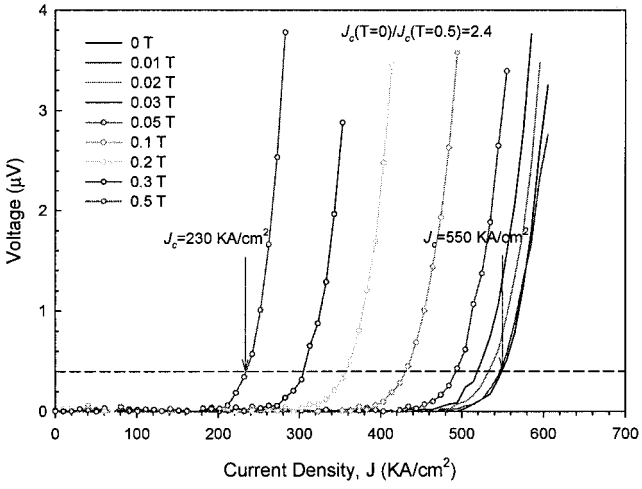

Fig. 7. Magnetic field dependence of J_c at 77 K for the YBCO film annealed for 30 min in humid furnace gas with magnetic field, H, applied parallel to the c-axis direction ($H//C_\perp$). The critical current density was decided by using a voltage criterion of 1 μV/cm.

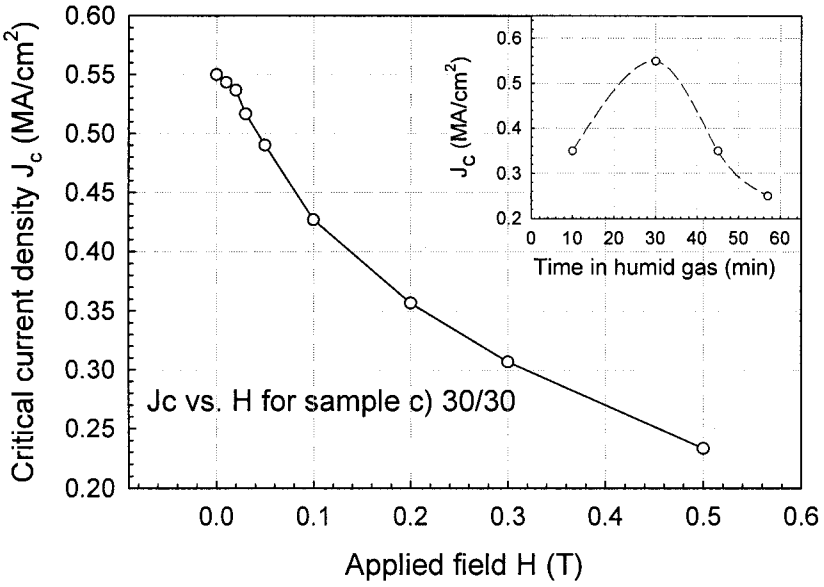

Fig. 8. Magnetic field dependence of J_c for samples annealed at 740°C in 180 ppm oxygen with 30 min wet-dwell. The inset shows the wet-dwell time dependence of the critical current density, indicating the highest current density arrived at 30-min dwell in humid furnace at 740°C.

experiment, both XRD θ–2θ scans (Fig. 1) and SEM (Fig. 6) do not show much *a*-axis-oriented material, the low current density cannot be attribute to 90° grain boundaries in this case. Another factor, the reaction between YBCO and CeO_2, may contribute to the low J_c in this experiment. Fig. 9 shows a typical RBS spectra of a YBCO film on CeO_2-buffered YSZ. No clear YBCO/CeO_2 boundary can be detected for samples treated with different wet-dwell times. An average thickness of ~200 nm based on Ba content and assuming fully dense YBCO was estimated from the RBS data. Due to the overlapping of the buffer layer and substrate peaks, it is difficult to get an accurate assessment of the stoichiometry. The extension of the tail of the barium peak to the low-energy part demonstrates that Ba atoms extend deep into the layer of CeO_2. The peaks of $BaCeO_3$ (111) and (200) in the X-ray θ–2θ scans indicate a reaction between YBCO and CeO_2 buffer during the high-temperature anneal at 740°C. Lastly, the ratio of Ortho-I, Ortho-II and tetragonal phases of YBCO may be limiting the transport J_c in these samples. In a recent work by Venkataraman *et al.*,[20] it is found using Raman spectroscopy that YBCO microdomains of differing oxygen contents exist in coated conductor samples and hence affect J_c significantly. Future work using detailed Raman spectroscopy studies is planned.

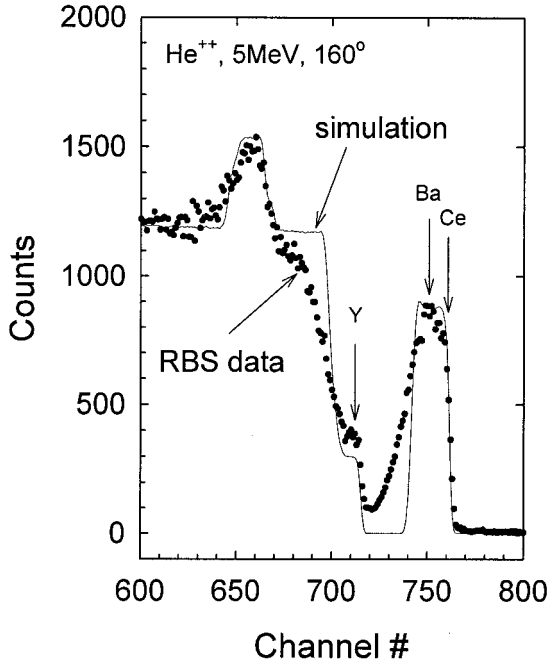

Fig. 9. RBS spectra of a YBCO film on CeO_2-buffered YSZ substrate, showing a typical energy spectra for the samples in this study. The RBS measurement was conducted at 5 MeV He^{2+} and a backscatter angle of 160°.

The correlations among the results from processing parameters in this experiment can be seen from the data of $T_c(R=0)$, ΔT_c, and J_c, in Table I. A marked degradation in T_c can be observed when YBCO films were annealed in humid atmosphere longer than 45 min or shorter than 30 min. Samples (b) and (c) have almost the same $T_c(R=0)$ value; however, the transition width ΔT_c tends to be broad for a longer dwell in humid furnace gas. For the samples annealed in wet furnace gas less than 30 min, the ρ vs *T* in the normal state is relatively straight and the extrapolation goes close to zero at 0 K. Also the ratio of ρ_{285}/ρ_{100} turns out the same (2.5) as the sample treated for 30 min and less in wet atmosphere, and the ratio of ρ_{285}/ρ_{100} seems comparable with the data reported by Feenstra *et al.*[21] High J_c values are associated with high T_c values and small transition width. High normal-state resistivity, a low T_c with broad transition, and a low J_c have been observed routinely for an extended hold (>30 mins) in humid gas in other sets of samples, indicating that water must play a big role in degrading the electrical properties in a YBCO film during high-temperature annealing.

The SEM top-view micrographs in Fig. 6 show the effect of the wet-dwell time during high-temperature annealing on the film morphology. The grains grew as large interconnected platelets that lie parallel to the surface. Smaller grains with spherical morphology, clearly visible in Fig. 6(a) and (b), decorate the surface of the platelets; also *a*-axis-oriented needle shaped grains are occasionally observed in these samples, which seems to be associated with the longer time in humid atmosphere. The *a*-axis-oriented grains are seldom observed on the films treated in shorter time in humid gas; for example, these features are not seen for the samples treated for 30 and 10 min in humid furnace gas (Fig. 6(c) and (d)). Other features such as pores, large voids (especially for longer exposure to water vapor, Fig. 6(a)), and irregularly shaped surface segregates are observed. The surface roughness of sample (c) appears to be lower than for samples processed under other conditions.

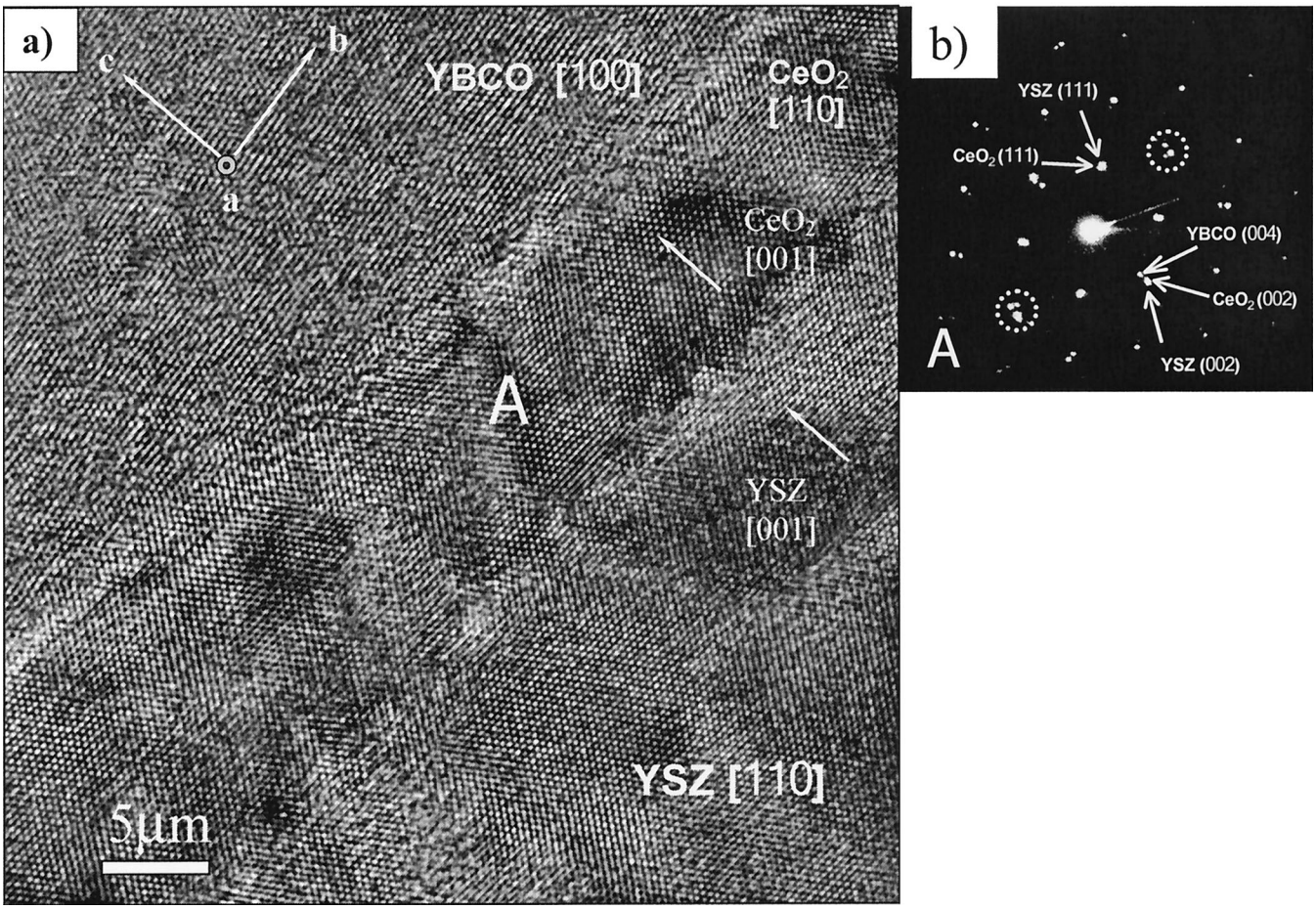

Fig. 10. HRTEM shows the interface zone of YBCO/CeO_2/YSZ. Epigrowth orientation was determined as YBCO (00*l*)//CeO_2 (00*l*)//YSZ(00*l*), YBCO [100]//CeO_2 [110]//YSZ [110]. A small tilt angle can be observed on the HRTEM image (a) and the SEADP (b).

Surface roughness increases when the wet-dwell time is off 30 min, especially for a longer hold in a humid furnace gas. The connectivity of the grains also degrades with an increased holding time in humid gas during high-temperature annealing. The average subgrain size is estimated to be 2–3 μm, which is comparable to those found in bulk materials. In addition to those samples discussed above, longer treatment over 60 min for 200-nm-thick YBCO films at 740°C in 180 ppm oxygen has been found to have a negative effect on the morphology as well as on electrical properties.

The wet-dwell time at the reaction temperature during the conversion has proved to have a tremendous influence on the final microstructure and the superconducting properties. We have found particularly that the porosity of the samples is strongly dependent on this parameter. The difference in residual porosity of these samples is easily seen in Fig. 6. While the sample prepared for 57 min in water vapor is extremely porous, especially at the subgrain boundaries, the type of porosity for holding shorter in humid gas, Figs. 6(c) and (d), is obviously different from those with longer wet-dwell, Figs. 6(a) and (b). The grain-boundary structure for sample (b) (wet-dwell for 45 min) shows an intermediate state between 30- and 57-min wet-dwelled samples. Because the total hold time for all the samples is the same (60 min), the porosity, especially holes at subgrain boundaries, is directly related to the exposure to water vapor. Clearly, water reacts with YBCO films at subgrain boundaries and the small misorientation at the subgrain boundaries seems to provide the driving force for this reaction. YBCO phase development when exposed to water vapor can be described as follows: $<$30 min, incomplete development; about 30 min, YBCO formation complete; $>$30 min, YBCO reacts with water and the film is degraded. It should be noted that the reaction of YBCO with water vapor might start soon after formation of the YBCO phase.

Figure 10 shows a cross-sectional HRTEM image and a SAD pattern taken in the vicinity of the interfaces of YBCO/CeO_2/YSZ for sample (c). As shown in the figure observed from the YBCO (100) direction, YBCO resembles a near single crystal with a slight tilt of about 3° relative to the buffer, observed both on the HRTEM and on the SAD pattern. A layer of about 10 nm of CeO_2 was observed with clear boundaries with YBCO film and YSZ substrate. This thickness is correlated to the time for the CeO_2 deposition in the RF sputtering system. The heteroepigrowth of the CeO_2 film on the YSZ surface and the YBCO film on the CeO_2 surface is illustrated by the HRTEM. A 45° rotation of YBCO (100) from CeO_2 (100) in this observation coincides with the result observed in the (113) pole figure in Fig. 4. With the help of SAD, the epitaxial growth feature was determined as YBCO (00*l*)//CeO_2 (00*l*)//YSZ (00*l*) and YBCO [100]//CeO_2 [110]//YSZ (110). As with the XRD analysis, the local HRTEM image does not show the existence of any $BaCO_3$ phase in the film, indicating that $BaCO_3$ might decompose completely at the conversion temperature in a humid atmosphere, or $BaCO_3$ is not an intermediate phase formed during burnout or in the heating of the high-temperature anneal. The existence of the reaction product $BaCeO_3$ shown in the XRD θ–2θ diffraction was not observed in Fig. 10, but we did find the existence of a $BaCeO_3$ phase in other places at the YBCO/CeO_2 interface. The formation of the $BaCeO_3$ phase is not spread out at the interface uniformly.

To further investigate the interface feature of YBCO/CeO_2/YSZ, a Bragg mask was used to filter the image. As illustrated in Fig. 11, both the YBCO/CeO_2 and CeO_2/YSZ interfaces are controlled by edge dislocations. The measured value of the misorientation angle, the tilted angle, for the YBCO/CeO_2 interface is about 3° up to the place observed. The mismatch between YBCO and CeO_2 is only about 1%, which will result in a tilt of

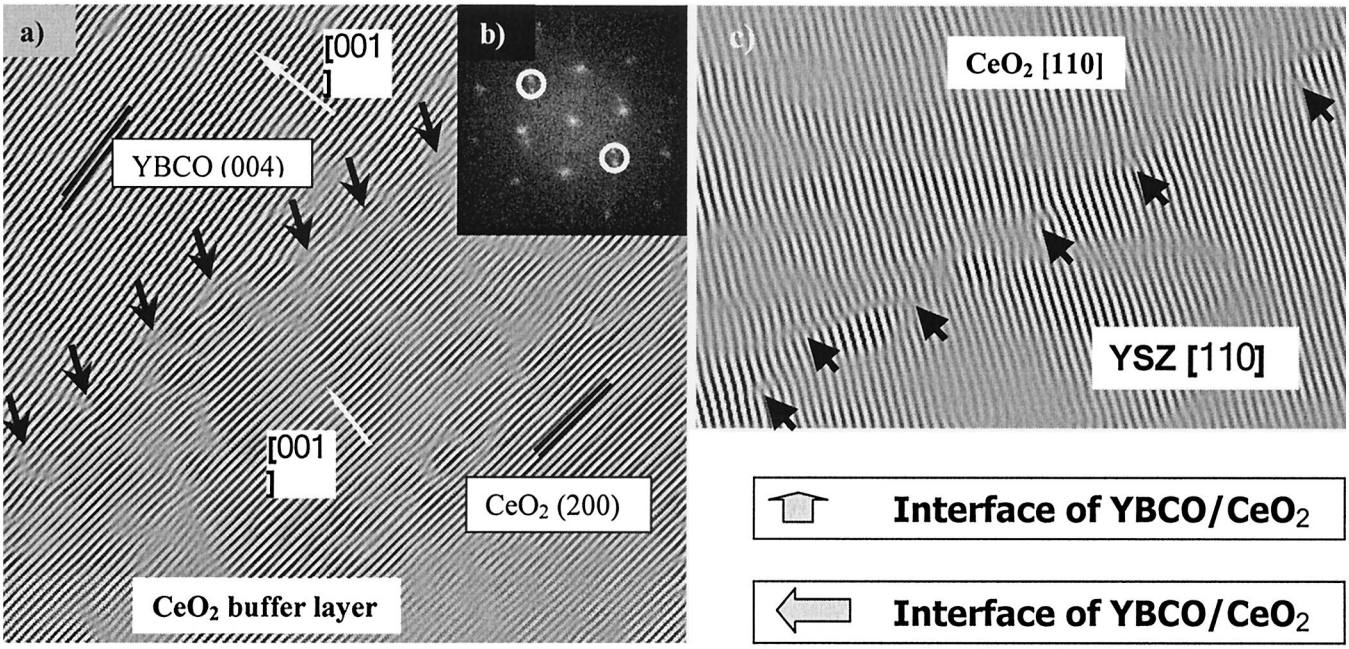

Fig. 11. Filtered image with Bragg mask indicating epigrowth and an edge dislocation feature at the interfaces of YBCO/CeO_2 (a) and CeO_2/YSZ (c). A tilt of YBCO (004) from CeO_2 (002) is shown on the SAD (b) by the circles.

about 1°, less than the measured tilt angle of about 3°. This means that though some of the stress is released at the interface of CeO_2/YSZ by edge dislocations, as shown in Fig. 11(c), most of the strain initiated by the stress at the interface of CeO_2/YSZ was carried by the CeO_2 layer and delivered to the interface of YBCO/CeO_2. This is reasonable as the thickness of the CeO_2 is only about 10 nm, much thinner than the YSZ substrate (0.5 mm). Accordingly the mismatch at the interface of YBCO/CeO_2 is mainly dominated by the mismatch of YBCO/YSZ (5%–6%), which can result in a tilt of about 3°. Hence, a relatively high density of edge dislocation was observed at the interface of YBCO/CeO_2.

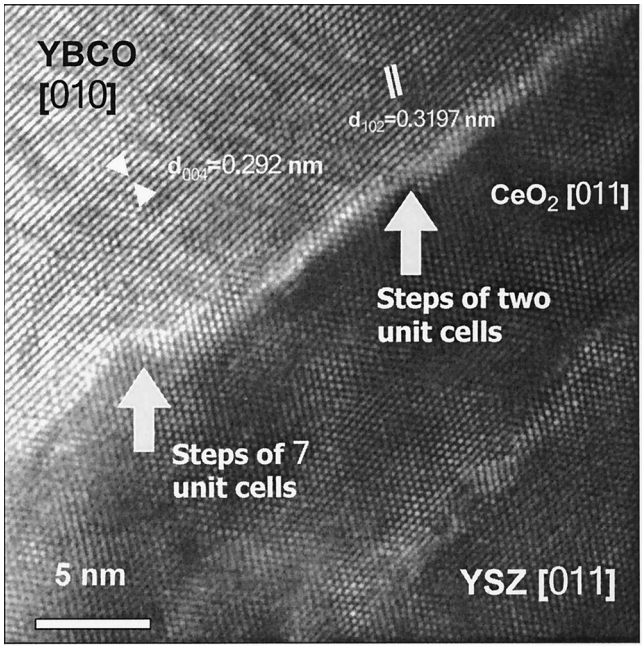

Fig. 12. HRTEM image of the interface of YBCO/CeO_2/YSZ. Small steps on the surface of the CeO_2 buffer layer were observed with the height of the couple of unit cells which may form the ideal position for the YBCO nucleation.

The nucleation mechanism for the fluorine-free method is not yet fully understood. In our experiment the epitaxial growth of the YBCO film demonstrated by XRD diffraction, HRTEM and SAD indicate that YBCO growth initially starts from interface of the precursor film and CeO_2. The steps observed on the CeO_2 surface are normally within the height of several unit cells, and they may provide ideal positions for YBCO nuclei, as shown in Fig. 12. The base of the steps is usually viewed as the place where the nucleation energy is less than that on a flat surface and thus favored for the nucleation. The traditional lateral growth models, for example, the layered growth model of Frank–Van der Merwe[22,23] and step-flow mechanism/step-mediated growth,[24–26] may be used to explain the YBCO epitaxial growth. But more evidence is needed before any solid conclusions be drawn on the nucleation mechanisms for the fluorine-free precursor derived YBCO films.

IV. Summary

A superconducting YBCO film with a thickness of 200 nm, $T_c(R=0)$ greater than 90 K and J_c (77 K, self-field) of 5.5×10^5 A/cm^2 was prepared by the fluorine-free metal organic deposition process. The dwell time in humid furnace gas during the high-temperature anneal had a strong effect on the surface morphologies and electrical properties of the YBCO films. The highest T_c and J_c were achieved for the film annealed for 30 min in humid atmosphere at 740°C in an oxygen partial pressure of 180 ppm. Degradation of the properties was observed for the samples treated for more than 30 min in humid atmosphere. Both XRD scans and TEM analysis show good epitaxial growth of YBCO films on CeO_2-buffered YSZ substrate, and the orientation relationship is YBCO (00*l*)//CeO_2 (00*l*)//YSZ (00*l*) and YBCO [100]//CeO_2 [110]//YSZ (110).

References

[1]C. E. Rice, R. B. Vandover, and G. J. Fisanick, "Preparation of Superconducting Thin-Films of $Ba_2YCu_3O_7$ by a Novel Spin-on Pyrolysis Technique," *Appl. Phys. Lett.*, **51** [22] 1842–44 (1987).

[2]M. E. Gross, M. Hong, S. H. Liou, P. K. Gallagher, and J. Kwo, "Versatile New Metalorganic Process for Preparing Superconducting Thin-Films," *Appl. Phys. Lett.*, **52** [2] 160–62 (1988).

[3]A. H. Hamdi, J. V. Mantese, A. L. Micheli, R. C. O. Laugal, D. F. Dungan, Z. H. Zhang, and K. R. Padmanabhan, "Formation of Thin-Film High-T_c Superconductors by Metalorganic Deposition," *Appl. Phys. Lett.*, **51** [25] 2152–54 (1987).

[4]P. Y. Chu and R. C. Buchanan, "Reactive Liquid-Phase Sintering of Solution-Derived $YBa_2Cu_3O_{7-x}$ Superconducting Thin-Films. 1. Ambient and Precursor Effects on BaO–CuO Liquid-Phase Formation," *J. Mater. Res.*, **8** [9] 2134–42 (1993).

[5]M. Paranthaman, "Non-Fluorine Based Solution Techniques To Grow Superconducting $YBa_2Cu_3O_{7-\delta}$ Films—A Review"; in *Next Generation HTS Conductors*. Edited by A. Goyal. Plenum Publishing Corp., London, U.K., 2002.

[6]A. Gupta, R. Jagannathan, E. I. Cooper, E. A. Giess, J. I. Landman, and B. W. Hussey, "Superconducting Oxide-Films with High Transition-Temperature Prepared from Metal Trifluoroacetate Precursors," *Appl. Phys. Lett.*, **52** [24] 2077–79 (1988).

[7]P. C. McIntyre, M. J. Cima, and M. F. Ng, "Metalorganic Deposition of High-J_c $Ba_2YCu_3O_{7-x}$ Thin Films from Trifluoroacetate Precursors onto (100) $SrTiO_3$," *J. Appl. Phys.*, **68** [8] 4183–87 (1990).

[8]A. Gupta, E. I. Cooper, R. Jagannathan, and E. A. Geiss, *Chemistry of High-Temperature Superconductors II*, p. 265. Edited by D. L. Nelson and T. F. George. American Chemical Society, Washington, D.C., 1988.

[9]A. Gupta, E. I. Cooper, R. Jagannathan, and E. A. Giess, pp. 265–79 in *Preparation of Superconducting Oxide Films from Metal Trifluoroacetate Solution Precursors*. ACS Symposium Series, Vol. 377. Edited by D. Larbalestier. American Chemical Society, Washington, D.C., 1988.

[10]J. A. Smith, M. J. Cima, and N. Sonnenberg, "High Critical Current Density Thick MOD-Derived YBCO Films," *IEEE Trans. Appl. Supercond.*, **9** [2] 1531–34 (1999).

[11]Y. A. Jee, B. Ma, V. A. Maroni, M. Li, B. L. Fisher, and U. Balachandran, "Texture Development and Superconducting Properties of $YBa_2Cu_3O_x$ Thin Films Prepared by a Solution Process in Low Oxygen Partial Pressure," *Supercond. Sci. Technol.*, **14** [5] 285–91 (2001).

[12]A. Goyal, D. P. Norton, J. D. Budai, M. Paranthaman, E. D. Specht, D. M. Kroeger, D. K. Christen, Q. He, B. Saffian, F. A. List, D. F. Lee, P. M. Martin, C. E. Klabunde, E. Hartfield, and V. K. Sikka, "High Critical Current Density Superconducting Tapes by Epitaxial Deposition of $YBa_2Cu_3O_x$ Thick Films on Biaxially Textured Metals," *Appl. Phys. Lett.*, **69** [12] 1795–97 (1996).

[13]A. Goyal, J. D. Budai, D. M. Kroeger, D. P. Norton, D. P. Christen, and E. D. Specht, U.S. Pat. No. 5 739 086, 1998.

[14]A. Goyal, J. D. Budai, D. M. Kroeger, D. P. Norton, D. P. Christen, E. D. Specht, and M. Paranthaman, U.S. Pat. No. 5 741 377, 1998.

[15]A. Goyal, J. D. Budai, D. M. Kroeger, D. P. Norton, E. D. Specht, and D. P. Christen, U.S. Pat. No. 5 898 020, 1999.

[16]T. Araki, Y. Takahashi, K. Yamagiwa, Y. Iijima, K. Takeda, Y. Yamada, J. Shibata, T. Hirayama, and I. Hirabayashi, "Firing Condition for Entire Reactions of Fluorides with Water Vapor in Metalorganic Deposition Method Using Trifluoro Acetate," *Physica C*, 2001. **357**, 991–94 (2001).

[17]S. Hirano, T. Hayashi, and M. Miura, "Preparation of $Ba_2YCu_3O_{7-\sigma}$ Thin Films with Preferred Orientation through an Organometallic Route," J. Am. Ceram. Soc., **73** [4] 885–88 (1990).

[18]F. Parmigiani, G. Chiarello, N. Ripamonti, H. Goretzki, and U. Roll, "Observation of Carboxylic Groups in the Lattice of Sintered $Ba_2YCu_3O_{7-y}$ High-T_c Superconductors," *Phys. Rev. [Sect.] B*, **36** [13] 7148–50 (1987).

[19]Y. Xu, A. Goyal, N. A. Rutter, D. Shi, M. Paranthaman, S. Sathyamurthy, P. M. Martin, and D. M. Kroeger, "Fabrication of High J_c $YBa_2Cu_3O_{7-\delta}$ Films Using a Fluorine-Free Sol Gel Approach. *J. Mater. Res.*, **18** [3] 677–81 (2003).

[20]K. Venkataraman, A. J. Kropf, C. U. Segre, Q. X. Jia, A. Goyal, B. W. Kang, S. Chattopadhyay, H. You, and V. A. Maroni, "Detection of Interfacial Strain and Phase Separation in $MBa_2Cu_3O_{7-x}$ Thin Films Using Raman Spectroscopy and X-ray Diffraction Space Mapping," *Physica C (Amsterdam)*, **402**, 1–16 (2004).

[21]R. Feenstra, T. B. Lindemer, J. D. Budai, and M. D. Galloway, "Effect of Oxygen-Pressure on the Synthesis of $YBa_2Cu_3O_{7-x}$ Thin Films by Post-deposition Annealing," *J. Appl. Phys.*, **69** [9] 6569–85 (1991).

[22]X. Zhu, G. C. Xiong, R. Liu, Y. J. Li, G. J. Lian, J. Li, and Z. Z. Gan, "The Growth Mechanism and Topography of Superconducting $YBa_2Cu_3O_{7-\delta}$ and BiSrCaCuO-2201 Films Studied by Scanning Tunneling Microscopy," *Physica C (Amsterdam)*, **216** [1–2] 153–59 (1993).

[23]D. L. Smith, *Thin-Film Deposition Principle and Practice*. Edited by D. L. Smith. McGraw-Hill, Inc., New York, 1995.

[24]Krug, J., "Origins of Scale Invariance in Growth Processes," *Adv. Phys.*, **46** [2] 139–282 (1997).

[25]L. Mechin, P. Berghuis, and J. E. Evetts, "Properties of $YBa_2Cu_3O_{7-\delta}$ Thin Films Grown on Vicinal $SrTiO_3$ (001) Substrates," *Physica C (Amsterdam)*, **302** [2–3] 102–12 (1998).

[26]S. Oda, H. Zama, and S. Yamamoto, "Atomic Layer Controlled Metalorganic Chemical-Vapor-Deposition of Superconducting $YBa_2Cu_3O_x$ Films," *J. Cryst. Growth*, **145** [1–4] 232–36 (1994). □